ЛВЭ

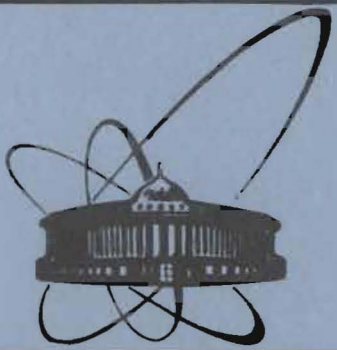

объединенный
институт
ядерных
исследований
дубна

E17-85-236

S.L.Drechsler, M.Bobeth

DIELECTRIC PROPERTIES OF TRANSPOLYACETYLENE.

The Macroscopic Longitudinal Dielectric Function of a Peierls-Fröhlich Semiconductor of Commensurability 2 within RPA

Submitted to "physica status solidi, (b)"

1985

2. THE MODEL

The actual crystal structure of trans-$(CH)_x$ according to the data of [17] is shown in fig.1a. To simplify the calculations we use as a model structure a quadratic lattice of equivalent chains (see fig.1b), where the area per chain is taken as the actual one. Using the data of Fincher et al. [17] one obtains the lattice constants $2a = 2.46$ Å, $b = 3.94$ Å and the volume of the unit cell Ω_0, i.e., the volume per C_2H_2 unit, $\Omega_0 = 2ab^2 = 38.27$ Å^3. Comparing the resulting bulk density (≈ 1.138 gcm^{-3}) with the density of real inhomogeneous films (≈ 0.4 gcm^{-3} [14]) a filling factor of one third can be estimated.

The model Hamiltonian proposed in [8] reads

$$\hat{H} = \sum_{\ell} \hat{H}_{\ell} + \hat{H}_{\perp}, \tag{2.1}$$

where $\hat{H}_{\ell}$ is the single-chain SSH-Hamiltonian [6] of the l-th chain:

$$\hat{H}_{\ell} = -t_0 \sum_{s,n} [1 + (-1)^n y] (c^{+}_{\ell,n,s} c_{\ell,n+1,s} + \text{h.c.}), \tag{2.2}$$

which describes in a TB-picture the behaviour of the π-electrons of the system under consideration (where one π-orbital per C-site, numbered by n, is provided and s is the spin index). The overall width of the whole π-band, $4t_0$ (usually to be taken $4t_0 \approx 10 \div 12$ eV) is chosen as the scaling energy of the considered problem. The Peierls gap between the filled valence band (π-band) and the empty conduction band (π^*-band) becomes in units of $4t_0$ a small parameter: $y = E_g/4t_0 \approx 0.14 \div 0.17 << 1$. To get some insight into the influence of an interchain coupling on the DF, a next neighbour hopping between chains has been added to (2.2)

$$\hat{H}_{\perp} = -t_{\perp} \sum_{\ell\ell',s,n} (c^{+}_{\ell,n,s} c_{\ell',n,s} + \text{h.c.}). \tag{2.3}$$

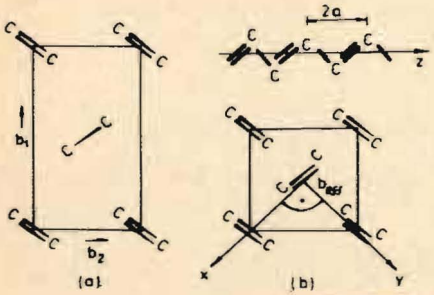

Fig.1. Schematic structure of transpolyacetylene (a) and simplified one (b) used in the calculation (b_1=7.32 Å, b_2 = =4.25 Å [17], b_{eff} = 3.94 Å).

Assuming the interchain hopping $t_\perp \ll t_0$ [18], the Bloch-wave function in the zeroth order in $t_\perp$ is given by

$$\Psi^{(n)}_{\vec{k}}(\vec{r}) = \frac{1}{\sqrt{N_E}} \sum_{\vec{R}} e^{i\vec{k}\vec{R}} \sum_{\nu=0}^{1} U^n_\nu(\vec{k}) \Phi_\nu(\vec{r} - \vec{R} - \nu\vec{a}), \tag{2.4}$$

where $n = 0,1$ stands for the conduction and valence bands, respectively, and $\Phi_\nu(\vec{r} - \vec{R} - \nu\vec{a})$ is the associated Wannier-function. The position of the unit cell is denoted by $\vec{R}$, $\vec{a}$ is the displacement vector between different sites of the same cell, and N_E means the number of unit cells. The coefficients $U^n_\nu(k)$ depend besides a phase factor only on the $\vec{k}$-component in chain direction $k_\parallel$ according to the relations:

$$\left.\begin{aligned} U^0_\nu &= \frac{1}{2}\left[(-1)^\nu \alpha(k_\parallel) - i\beta(k_\parallel)\right] e^{i\nu\vec{k}\vec{a}} \\ U^1_\nu &= \frac{1}{2}\left[\alpha(k_\parallel) - i(-1)^\nu \beta(k_\parallel)\right] e^{i\nu\vec{k}\vec{a}} \end{aligned}\right\} \quad \nu = 0,1\,, \tag{2.5}$$

where

$$\left.\begin{aligned} \alpha(k_\parallel) &= \{[s_\parallel(k_\parallel) + \cos k_\parallel a]/s_\parallel(k_\parallel)\}^{1/2} \\ \beta(k_\parallel) &= \mathrm{sgn}(\sin k_\parallel a)\{[s_\parallel(k_\parallel) - \cos k_\parallel a]/s_\parallel(k_\parallel)\}^{1/2} \end{aligned}\right\} \tag{2.6}$$

$$s_\parallel(k_\parallel) = [1 - k^2 \sin^2 k_\parallel a]^{1/2}, \quad k^2 = 1 - \gamma^2, \tag{2.7}$$

and a is the projection of $\vec{a}$ on the chain axis. Note, that the notation on (2.5-6) and (3.5) has been changed and differs from the analogous expressions in [8] by the phase factor and the proper prefactor $(N_E)^{-1/2}$ instead of $(2N_E)^{-1/2}$ corresponding to the Hanke-Sham calculation scheme [16]. The eigenvalues of the Hamiltonian (2.1) in the first order of $t_\perp$ are given by

$$\left.\begin{aligned} E_\nu(\vec{k}) &= (-1)^\nu 2t_0 s_\parallel(k_\parallel) + 2t_\perp(\vec{k}_\perp); \quad \nu = 0,1, \\ s_\perp(\vec{k}_\perp) &= (1/2) \sum_{\ell'} e^{i\vec{k}_\perp \vec{R}_{\ell'}}, \end{aligned}\right. \tag{2.8}$$

where the sum has to be taken over nearest neighbour chains.

3. THE MACROSCOPIC LONGITUDINAL DIELECTRIC FUNCTION (MLDF)

Usually, the MLDF $\epsilon(\vec{q}, \omega)$ is expressed by the density correlation function $\hat{\chi}(\vec{q}, \omega)$

$$\epsilon(\vec{q}, \omega) \equiv [\epsilon^{-1}_{micr}(\vec{q}, \vec{q}; \omega)]^{-1} = \epsilon_\infty [1 - v(q)\hat{\chi}(\vec{q}, \omega)], \tag{3.1}$$

where according to [16,18] $\hat{\chi}$ is written in terms of the Wannier-function Φ_ν (mentioned in sect.2), the form factors of the charge density A_s and the screening matrix $\hat{S}_{ss'}$:

$$\hat{\chi}(\vec{q}, \omega) = \sum_{ss'} A_s(\vec{q}) \hat{S}^{-1}_{ss'}(\vec{q}, \omega) A^*_{s'}(\vec{q}), \tag{3.2}$$

$$A_s(\vec{q}) = \int d^3\vec{r}\, \Phi_\nu(\vec{r} - \nu\vec{a})\, e^{-i\vec{q}\vec{r}}\, \Phi_{\nu'}(\vec{r} - \vec{R} - \nu'\vec{a}), \tag{3.3}$$

$$\hat{S}^{-1}_{ss'}(\vec{q}, \omega) = \hat{N}^{(0)}_{ss'}(\vec{q}, \omega)\{\hat{1} - [\hat{V} - \frac{1}{2}\hat{V}_{ex}]\hat{N}(\vec{q}, \omega)\}^{-1}_{s's}, \tag{3.4}$$

where s denotes the composite matrix index $s \equiv (\vec{R}, \nu, \nu')$. At low temperatures $k_B T \ll E_g$ the polarization bubble $N^{(0)}_{ss'}(\vec{q}, \omega)$ is

$$N^{(0)}_{s_1, s_2}(\vec{q}, \omega) = \frac{2}{N_E} \sum_{n \neq n'} U^{n*}_{\nu_1}(\vec{k}) U^{n'}_{\nu'_1}(\vec{k} + \vec{q})\, e^{i(\vec{k}+\vec{q})(\vec{R}_1 - \vec{R}_2)} \times$$
$$\times\, U^n_{\nu_2}(\vec{k}) U^{n'}_{\nu'_2}(\vec{k} + \vec{q}) \cdot \left[\frac{f(n', \vec{k}+\vec{q}) - f(n, \vec{k})}{E_{n'}(\vec{k}+\vec{q}) - E_n(\vec{k}) - \hbar\omega - i\delta}\right]. \tag{3.5}$$

The Fourier-component of the bare Coulomb potential in (3.1) at long-wavelengths compared with the strand radius is certainly (see the discussions in [20,21]) $v(q) = 4\pi e^2/(\Omega_0 \epsilon_\infty q^2)$, where ϵ_∞ describes an isotropic background dielectric contribution resulting from electronic transitions ω_R at sufficiently high frequencies $\hbar\omega_R \gtrsim 4t_0$ much higher than the frequency region of our interest (e.g., interband plasmons, see below). As a typical value for an organic solid we take $\epsilon_\infty \approx 2 \div 3$. Like in [8] in the first step the overlap between neighbouring sites in calculating A_s (3.3) as well as the Coulomb matrix $\hat{V}_{ss'}$ and the exchange correction $\hat{V}_{ex,ss'}$ in (3.4) are neglected (their influence will be considered in a subsequent paper). Then, we get

$$A_{\vec{R}, \nu, \nu'} = e^{-i\vec{q}\vec{a}\nu} \delta_{\vec{R}, 0}\, \delta_{\nu\nu'} \tag{3.6}$$

and $\hat{\chi}(\vec{q}, \omega)$ becomes

$$\hat{\chi}_{RPA}(\vec{q}, \omega) = \frac{1}{2N_E \Omega_0 t_0} \sum_{\vec{k}} \left(\frac{1}{D_1} - \frac{1}{D_0}\right) W_0(\vec{q}, \vec{k}), \tag{3.7}$$

where the dimensionless notation

$$\left.\begin{aligned} D_1 &= \tilde{E}_1(\vec{k} + \vec{q}) - \tilde{E}_0(\vec{k}) - 2\tilde{\omega}, \quad D_0 = \tilde{E}_0(\vec{k} + \vec{q}) - \tilde{E}_1(\vec{k}) - 2\tilde{\omega} \\ \tilde{E}_\nu(\vec{k}) &= (-1)^\nu s_\parallel(k_\parallel) + (t_\perp/t_0) s_\perp(\vec{k}_\perp), \quad \nu = 0,1, \quad \tilde{\omega} = \hbar\omega/4t_0 \end{aligned}\right. \tag{3.8}$$

has been introduced. In the zeroth order in $t_\perp$ the matrix ele-

ment $W_0(\vec{q}, \vec{k})$ in (3.7) becomes a function of $k_\parallel$ and $q_\parallel$ only

$$W_0(q_\parallel, k_\parallel) = 1 - \frac{\cos k_\parallel a \cos(k_\parallel + q_\parallel)a + y^2 |\sin k_\parallel a \cdot \sin(k_\parallel + q_\parallel)a|}{s_\parallel(k_\parallel + q_\parallel)\, s_\parallel(k_\parallel)}. \quad (3.9)$$

In the long-wavelength limit we obtain

$$W_0(q_\parallel, k_\parallel) = 0.5(q_\parallel a)^2 y^2 / s_\parallel^4(k_\parallel) \quad \text{for} \quad q_\parallel a \ll 1, \quad (3.10)$$

which differs from the corresponding expression in [8] (formula (18)) by the exponent of $s_\parallel$ equal to 4 instead of 1. The $t_\perp$-dependence of $\epsilon(\vec{q}, \omega)$ via W_0 is expected to be weak and will be neglected, whereas for a qualitative discussion its influence on $\mathrm{Im}\,\epsilon(\vec{q}, \omega)$ via the denominator D_0 (eq.(3.8)) will be taken into account.

Otherwise the influence of the interchain coupling $t_\perp$ becomes negligible and the MLDF reads

$$\epsilon(\vec{q}, \omega) = \epsilon_\infty - C \int_{-\pi/2}^{\pi/2} d(k_\parallel a)(1/D_1 - 1/D_0) W_0(q_\parallel, k_\parallel)/(qa)^2, \quad (3.11)$$

where

$$C = (2e^2/t_0 a)\cdot(a^3/\Omega_0) \equiv (\hbar\omega_{p\ell})^2 \epsilon_\infty/(4t_0)^2,$$
$$\omega_{p\ell}^2 = 8e^2 \mathfrak{N} v_F/(\epsilon_\infty \hbar), \quad v_F = 2t_0 a/\hbar, \quad (3.12)$$

and $\omega_{p\ell}$ means the plasma frequency of the corresponding quasi-1D-metal with the area density of chains $\mathfrak{N}$ [21]. From the data referred to in sect.2 we obtain for polyacetylene $C \approx 0.45$. Note that (3.11) is essentially the Ehrenreich-Cohen formula in the extreme TB-limit for noninteracting chains.

4. EXPLICIT RESULTS AND DISCUSSION

4.1. The long wavelength limit. For $q_\parallel a \ll 1$ the integrals in (3.11) can be calculated analytically (compare fig.2):

$$\mathrm{Re}\,\epsilon(0, \omega) = \epsilon_\infty + \frac{C y^2 \cos^2\Theta}{\bar{\omega}^2}\left[\frac{\Pi(k/(1-\bar{\omega}^2), k)}{1-\bar{\omega}^2} - \frac{E(k)}{y^2}\right], \quad (4.1)$$

$$\mathrm{Im}\,\epsilon(0, \omega) = \begin{cases} \frac{\pi}{2} C y^2 \cos^2\Theta\, \omega^{-3} (\bar{\omega}^2 - y^2)^{-1/2} (1-\bar{\omega}^2)^{-1/2} & \text{for } y \le \bar{\omega} \le 1 \\ 0 \quad \text{otherwise,} \end{cases} \quad (4.2)$$

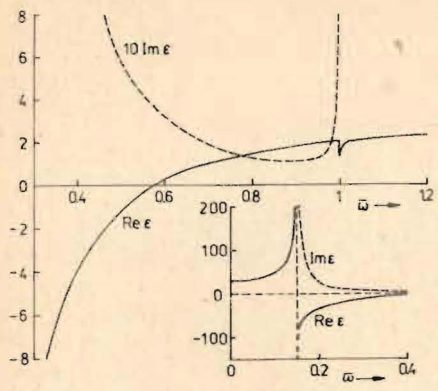

Fig. 2. $\mathrm{DF}\,\epsilon(0, \omega)$ *versus frequency* ($\bar{\omega} = \omega/4t_0$, $\epsilon_\infty = 3$, $y = E_g/4t_0 = 0.15$, $\cos\Theta = 1$, $C = 0.9$).

where $k = (1 - y^2)^{1/2}$ and Θ is the angle between $\vec{q}$ and the chain direction. Π and E denote the complete elliptic integrals of the third and second kind (for the definition of Π see [19]). Eqs.(4.1-2) fulfil the condition $\epsilon(\omega) = -\epsilon^*(-\omega)$ in contrast to [8], where the factor ω^{-3} in $\mathrm{Im}\,\epsilon(0, \omega)$ was lost. This factor and the square-root singularity at the gap frequency have been obtained by several authors [6,7,9-13] although the numerical prefactors differ for each treatment. In these works the dipole approximation and (or) a simplified linearized electronic dispersion law for the undimerized case were used. The latter is valid only for frequencies lower or near the gap, i.e., $\bar{\omega} \lesssim y \ll 1$. The absence of the singularity at the upper edge of the interband transitions (IBT), i.e., at $\bar{\omega} = 1$, is possibly connected with the difference of the longitudinal and transverse dielectric functions for crystals of noncubic symmetry [16,24] and the mentioned above linearization of the electronic structure.

Explicit expressions for $\mathrm{Re}\,\epsilon(0, \omega)$ for the quasi-1D-TB-semiconductor with commensurability 2 are given, to our knowledge, only in the work of Schulz [10] in the dipole approximation. According to the above given statement we get similar behaviour at low frequencies $\bar{\omega} \lesssim y$ and different one at high frequencies $\bar{\omega} \gtrsim 1$. According to the singularities of $\mathrm{Im}\,\epsilon(0, \omega)$ connected with the 1D-bandstructure, $\mathrm{Re}\,\epsilon(0, \omega)$ possesses square root singularities at the outsides of both IBT edges, i.e., at $\bar{\omega} \to y - 0$ and $\bar{\omega} \to 1 + 0$:

$$\mathrm{Re}\,\epsilon(0, \bar{\omega} \to y - 0) = \epsilon_\infty + \frac{C\cos^2\Theta}{k}\left[\frac{\pi(2y)^{-3/2}}{(y-\bar{\omega})^{1/2}} + K - \frac{Ek}{y^2}\right] \to +\infty,$$
$$\mathrm{Re}\,\epsilon(0, \bar{\omega} \to 1 + 0) = \epsilon_\infty - C\cos^2\Theta\left[\frac{\pi}{4k} y^2 (\bar{\omega}^2 - 1)^{-1/2} - \bar{\omega}^{-2}\right] \to -\infty, \quad (4.3)$$

where $K \equiv K(k)$ denotes the complete elliptic integral of the first kind (hereafter the k-dependence of the elliptic integrals will be omitted), whereas at the insides of the ITB edges $\mathrm{Re}\,\epsilon(0, \omega)$ remains finite:

$$\mathrm{Re}\,\epsilon(0,\bar{\omega}\to y+0)=\epsilon_\infty+C\cos^2\Theta\,(-2E/y^2+K+E)/k^2, \tag{4.4}$$

$$\approx\epsilon_\infty-2C\cos^2\Theta/y^2 \quad \text{for} \quad y\ll 1, \tag{4.5}$$

$$\mathrm{Re}\,\epsilon(0,\bar{\omega}\to 1-0)=\epsilon_\infty-C\cos^2\Theta\,(E+y^2(F-K)/k^2), \tag{4.6}$$

$$\approx\epsilon_\infty-C\cos^2\Theta \quad \text{for} \quad y\ll 1. \tag{4.7}$$

At very high frequencies $\bar{\omega}\gg 1$ or for $y\to 0$ we get quasimetallic behaviour

$$\mathrm{Re}\,\epsilon(0,\bar{\omega}\gg 1)=\epsilon_\infty(1-E\omega_{p\ell}^2\cos^2\Theta/\omega^2), \tag{4.8}$$

$$\approx\epsilon_\infty(1-\omega_{p\ell}^2\cos^2\Theta/\omega^2) \quad \text{for} \quad y\ll 1, \tag{4.9}$$

in agreement with the well-known result for the quasi-1D-metal [20,22]. Finally, at low frequencies $\bar{\omega}\ll y$ we have

$$\mathrm{Re}\,\epsilon(0,\bar{\omega}\ll y)=\epsilon_\infty+(2C\cos^2\Theta/3)(E/y^2-E-K/2), \tag{4.10}$$

$$\approx\epsilon_\infty+(2C/3y^2)\cos^2\Theta \quad \text{for} \quad y\ll 1. \tag{4.11}$$

The static value $\epsilon_\parallel$ for polyacetylene becomes $\epsilon_\parallel(0,0,\Theta=0)=\epsilon_\parallel\approx\epsilon_\infty+13.3\approx 15\div 16$ almost in agreement with [8]. This value seems to be somewhat enhanced in comparison with the usual accepted value derived from optical measurements [3]. However since the optical wavelengths are large compared to characteristic lengths of inhomogeneties of real $(CH)_x$-films, the optical data actually deal with a quite smaller effective dielectric constant resulting from the average over the volume and fibres orientation.

Let us now consider the zeroes of $\mathrm{Re}\,\epsilon(0,\omega)=0$ which are closely related to the plasmon energy given by the peak of the loss function $P(\omega)=-\mathrm{Im}\,1/\epsilon(\omega)$. Requiring different signs of (4.5) and (4.7) a simple condition for the occurrence of an interband plasmon can be obtained

$$1<\epsilon_\infty/(C\cos^2\Theta)<2/y^2 \tag{4.12}$$

which is fulfilled for $C\approx 0.45$ for a wide range of angles Θ. Hence, for films with more or less oriented fibres the peak of the measured averaged loss function $\langle P(\omega)\rangle_\Theta$ (see [15]) should be shifted to lower frequencies compared to the case $\Theta=0$. From (4.5) and (4.7) the position of the plasmon peak in $(CH)_x$ can be estimated in a crude manner by $\hbar\omega_{p\ell}^{sc}<4t_0(C/\epsilon_\infty)^{1/2}\sim(4\div 4.5)\,a^{1/2}$ eV and $1<a<2$ in good agreement with the experimental value of about 4 eV at $q=0.1$ Å^{-1}. (Some peculiarities at lower q-values found in [2] are discussed in [15]). Comparing (4.12) and (4.9) we

find that the plasmon frequency $\omega_{p\ell}^{sc}$ of the Peierls-Fröhlich semiconductor is somewhat enhanced compared to the undimerized metallic system $\omega_{p\ell}$:

$$\omega_{p\ell}^2<\omega_{p\ell}^{2\,sc}<a\,\omega_{p\ell}^2 \quad \text{with} \quad 1<a<2. \tag{4.13}$$

By using (4.11) $\omega_{p\ell}^{sc}$ can be related to the static dielectric constant $\epsilon_\parallel(0)$ by

$$1<1.5(\hbar\omega_{p\ell}^{sc}(\Theta=0))^2(\epsilon_\parallel(0)/\epsilon_\infty-1)^{-1}\,E_g^{-2}<a<2. \tag{4.14}$$

By comparing the limits (4.3) and (4.9) a further zero $\hbar\omega_{p\ell}^{(+)}$ is found very close to the upper edge of the interband transitions:

$$\hbar\omega_{p\ell}^{(+)}\approx 4t_0[1+(\pi/4)^2C^2y^4(k(\epsilon_\infty-C))^{-2}].$$

However, this solution seems to be an artifact of our model since at these frequencies additional electronic transitions and damping effects (compare fig.3 [14]) have to be taken into account explicitly.

4.2. The imaginary part of the DF at finite wave vectors.

The imaginary part of the DF is determined by the zeroes of D_0 in eq.(3.8) with respect to $k_\parallel$

$$\omega^*=\bar{\omega}-(t_\perp/2t_0)[s_\perp(\vec{k}_\perp+\vec{q}_\perp)-s_\perp(\vec{k}_\perp)]=(s_\parallel(k_\parallel+q_\parallel)+s_\parallel(k_\parallel))/2. \tag{4.15}$$

At first we discuss the limit $t_\perp\to 0$. From(4.15) simple analytical expressions for the upper and lower boundaries for $\mathrm{Im}\,\epsilon(q_\parallel,\omega)$ unequal zero in the $(\bar{\omega},q_\parallel)$- plane can be derived analyzing the first and second derivatives of (4.15) with respect to $k_\parallel$ (see fig.3). Thus, the upper boundary $\bar{\omega}_u(q_\parallel)$ consists of the curves AB and BC given by

$$\bar{\omega}_u(q_\parallel)=\begin{cases} s_\parallel(q_\parallel a/2) & \text{for} \quad q_\parallel a\le\pi/2, \quad \text{i.e. for AB} \\ s_\parallel(q_\parallel a/2-\pi/2) & \text{for} \quad \pi/2\le q_\parallel a\le\pi, \quad \text{i.e. for BC} \end{cases} \tag{4.16}$$

The lower boundary $\bar{\omega}_\ell(q_\parallel)$ is given by three curves:

$$\bar{\omega}_\ell(q_\parallel)=\begin{cases} s_\parallel(q_\parallel a/2-\pi/2) & \text{for} \quad 0\le q_\parallel a\le q_\parallel^c a, \quad \text{i.e. for DE} \\ 0.5x(x-y)^{-1/2} & \text{for} \quad aq_\parallel^c\le q_\parallel a\le\pi-q_\parallel^c a, \text{i.e. for EF} \\ s_\parallel(q_\parallel a/2) & \text{for} \quad \pi-q_\parallel^c a\le q_\parallel a\le\pi, \quad \text{i.e. for FG} \end{cases} \tag{4.17}$$

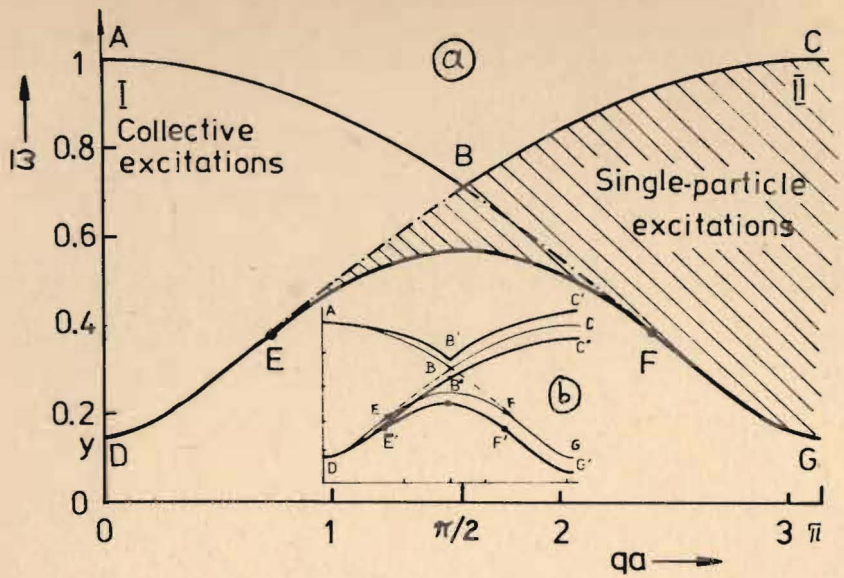

Fig. 4. Absorption region due to interband transitions for $\vec{q}_\perp = 0$ (or $t_\perp = 0$). (a). This region is sketched for $t_\perp \neq 0$ and $\vec{q}_\perp \parallel \vec{e}_x$ (or $\vec{e}_y$) in (b).

where

$$aq_\parallel^c = \arccos[(1-y)/(1+y)],$$

$$x = 0.5(1+y)\sin q_\parallel a \{(1+y)\sin q_\parallel a + [(1+y)^2 \sin^2 q_\parallel a - 4y]^{1/2}\}. \qquad (4.18)$$

It turns out that $\mathrm{Im}\,\epsilon(q, \omega)$ vanishes at the lines AB and FG caused by the behaviour of the matrix element $W_0(q_\parallel, k_\parallel)$, whereas at the other lines it tends to infinity:

$$\mathrm{Im}\,\epsilon(q, \omega) \sim \begin{cases} (\bar{\omega} - \bar{\omega}_l(q_\parallel))^{-1/2} & \text{near DF and EF} \\ (\bar{\omega}_u(q_\parallel) - \bar{\omega})^{-1/2} & \text{near BC and EB,} \end{cases} \qquad (4.19)$$

where the curve EB is given by eq.(4.16) continued to $aq^c \leq q_\parallel a \leq \pi/2$. Approaching from (4.19) and (4.2) we find that the lower ITB-edge shows strong dispersion in agreement with the statement of Ritsko [1]. At momenta higher than $q^c_\parallel$ (eq.(4.18)) it splits into two singularities where the lower one vanishes for $\pi - q^c_\parallel a < aq_\parallel < \pi$. Note that there is no branching point $(q^c_\parallel, \sqrt{y})$ in the sketch given by Ritsko (fig.7 of [1]). At the upper IBT-edge along the line AB the imaginary part goes to zero, but for small wave vectors a maximum appears near the edge which

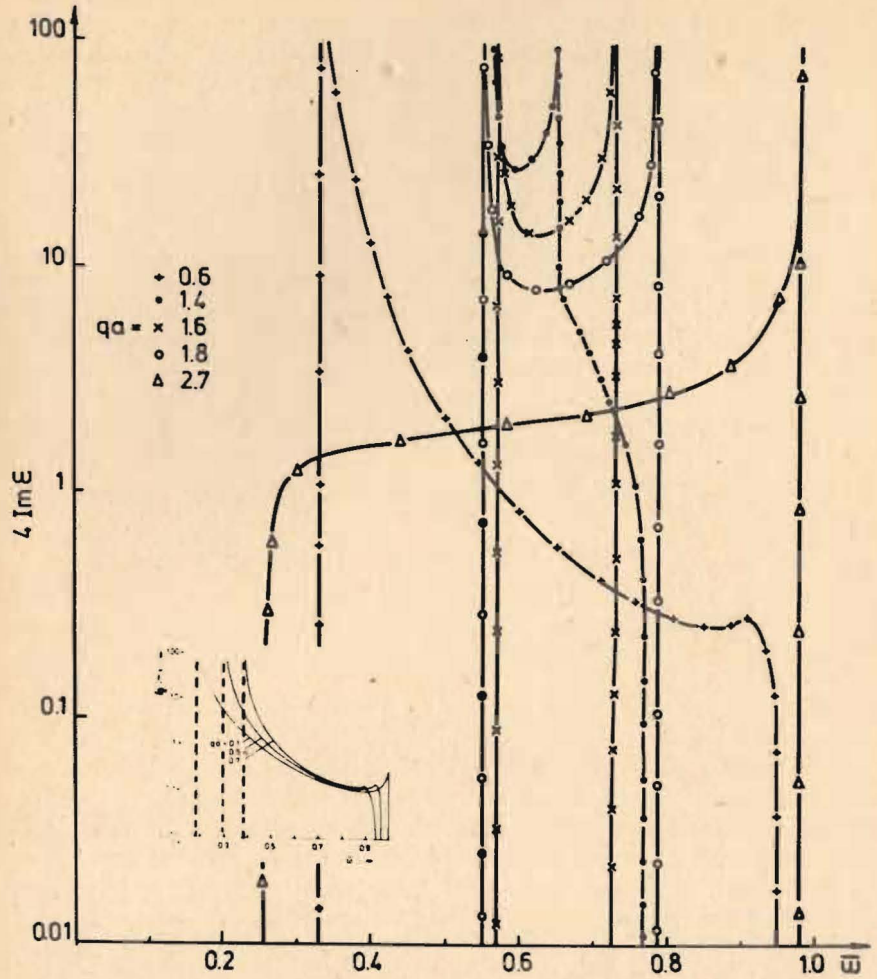

Fig. 4. Imaginary part of the DF versus frequency for different wave vectors (C = 0.45).

becomes a singularity in the limit $q \to 0$, $\bar{\omega} \to 1$. In the metallic limit $y \to 0$ the branching point $(q^c_\parallel, \sqrt{y})$ is displaced to the origin of the $(q_\parallel, \bar{\omega})$-plane and all the absorption above the line DBC disappears completely. The remaining region bounded by this line and DEFG becomes the well-known single-particle excitation spectrum of the quasi-1D-TB-metal (see [21]). The corresponding region (II) for the semiconductor could be denoted analogously (as it was done by Ritsko) if it is considered from the point of view of the loss function $P(q, \omega)$ because there are no sharp peaks there and $-\mathrm{Im}\,1/\epsilon(q, \omega)$ varies smoothly between the lines

EFG and EBC. In contrast with the region (II) in (I) occurs a plasmon peak, i.e., a collective excitation which however possesses even within the RPA a finite width due to single particle IBT excitations in contrast with the metallic case, where it is a delta-function. Note some incorrectness of the mentioned feature of Ritsko near the zone boundaries (i.e., at $q = 0$ and $aq = \pi$) where nearly linear dispersion instead of quadratic one was sketched.

Since the analytical expressions for $\mathrm{Im}\epsilon(q, \omega)$ take voluminous form, we do not quote them and refer the reader to fig.4.

Now let us briefly investigate the influence of the interchain coupling $t_\perp$ on the lines considered above. In the simplest case $\vec{q}_\perp = 0$ there is no influence at all and we return to the mentioned square-root singularities. If $\vec{q}_\perp$ is directed along the x- or y-axis the corresponding integration over $k_x(k_y)$ in (3.7) of the leading term of $\mathrm{Im}\epsilon(q_\parallel, q_x, 0, \omega)$ yields an incomplete elliptic integral of the first kind which possesses logarithmic singularities of the type

$$\mathrm{Im}\epsilon(q_\parallel, q_x, 0, \omega) \sim \begin{cases} \ln \dfrac{1}{|\bar{\omega}_{(-)} - \bar{\omega}|} & \text{near DE' and E'F'} \\ \ln \dfrac{1}{|\bar{\omega}_{(+)} - \bar{\omega}|} & \text{near B''C'' and E''B'',} \end{cases} \tag{4.20}$$

where

$$\bar{\omega}_{(\pm)}(\vec{q}) = \bar{\omega}_{u(\ell)}(\vec{q}_\parallel) - \delta\bar{\omega}(\vec{q}_\perp), \quad \delta\bar{\omega}(\vec{q}_\perp) = \frac{1}{2}(t_\perp/t_0)|\sin q_x b/2|. \tag{4.21}$$

After similar considerations for the other lines, one can summarize that the symmetric (with respect to the mirror line $q_\parallel a = \pi/2$) butterfly of fig.3 for finite interchain coupling and transverse momentum along one of the axes will be deformed into an "asymmetric" one which is given by eq.(4.21) and the replacement

$$\bar{\omega}_u(\vec{q}) = \bar{\omega}_u(q_\parallel) + \delta\bar{\omega}(\vec{q}_\perp) \quad \text{for AB' and B'C'.} \tag{4.22}$$

Thus DE''B''C'' becomes an inner line where $\mathrm{Im}\epsilon(\vec{q}, \omega)$ possesses a symmetric two-side logarithmic singularity whereas at the lower side the singularity occurs at one side (approaching from above) only. At the upper line AB'C' $\mathrm{Im}\epsilon(\vec{q}, \omega)$ vanishes now. For an arbitrary $\vec{q}_\perp$-direction all singularities disappear and sharp finite peaks remain. In all cases discussed above a finite $q_\parallel$-component was supposed otherwise $\mathrm{Im}\epsilon(\vec{q}, \omega)$ vanishes in our approach. The change of the singular behaviour of $\mathrm{Im}\epsilon(\vec{q}, \omega)$ for different $\vec{q}$-directions is analogous to the well-known van-Hove singularities of the density of states in dependence on the dimensionality of the dispersion law.

The peculiarities of the $\vec{q}$-dependence of the DF can be used in principle to determine the electronic parameters t_0 and $t_\perp$ from measurements of the loss function $P(\vec{q}, \omega)$ (see [15]) by introducing a new DF $\tilde{\epsilon}(q, \omega)$ the imaginary part of which is given by

$$\mathrm{Im}\tilde{\epsilon}(q, \omega) = P(q, \omega)/(P^2(q, \omega) + R^2(q, \omega)),$$

where R is the Kramers-Kronig transform of P. This function reflects to some extent the singularities of $\mathrm{Im}\epsilon(\vec{q}, \omega)$. The splitting of the low frequency peak in our model occurs at $q \gtrsim q_\parallel^c \approx 0.6\ \text{Å}^{-1}$ (for $y = 0.15$), whereas in the data of Ritsko [1] a much stronger splitting can be seen beginning from somewhat lower momenta $q \approx 0.5 \div 0.55\ \text{Å}^{-1}$. Using, e.g., the expression for the line EB (eq.(4.16)) one finds

$$t_0 = (\omega - 4)\ s\ (q_\parallel a \cdot 2 - \pi/2) \approx 2.72\ \text{eV},$$

(taking $\omega = 4.77$ eV, $y = 0.15$ and $q = 0.7\ \text{Å}^{-1}$ for the upper peak, see fig.2 of [1]) in fairly good agreement with the commonly used value $t_0 \approx 2.5$ eV. Carrying out experiments on monocrystals (not available at present) one could estimate $t_0/t_\perp$ from the singularity shift given by eq.(4.20).

4.3. The real part of the DF at finite wave vectors. Using the Kramers-Kronig relations one can quantitatively conclude from the singular behaviour of $\mathrm{Im}\epsilon(q, \omega)$ for $t_\perp = 0$ that $\mathrm{Re}\epsilon(q, \omega)$ possesses positive square root singularities approaching the line DEF from below, whereas the limit from above remains finite(negative).For $t_\perp \neq 0$ and $\vec{q}_\perp \parallel \vec{e}_x$ a logarithmic singularity is obtained and for arbitrary $\vec{q}_\perp$-direction the singularity vanishes. Approaching from above the lines EB and BC $\mathrm{Re}\epsilon(q, \omega)$ behaves in an analogous manner. On the other hand at very high frequencies $\mathrm{Re}\epsilon(q, \omega)$ is positive for arbitrary q-values. Thus, the interband plasmon given by the equation $\mathrm{Re}\epsilon(q, \omega) = 0$ cannot intersect the lines EB and BC and therefore the plasmon is never Landau damped, in agreement with the statement in [21] for the quasi-1D-metallic-TB-case. From the RPA-result (3.11) obtained for a monocrystal follows that there is always a region at low momenta with a quadratic q-dependence in contrast to the statement of [14,1], although the dispersion law quickly tends to a quasi-linear one for higher momenta.This seems to be in conflict with the experimental findings of [1,2]. We shall discuss this problem in connection with the loss function in our forthcoming paper [15]. The results of our numerical calculations for $\mathrm{Re}\epsilon(q, \omega)$ are shown in fig.5.

For some applications the static limit $\epsilon(q, 0)$ is also of interest. The corresponding curves are shown in fig.6 for dif-

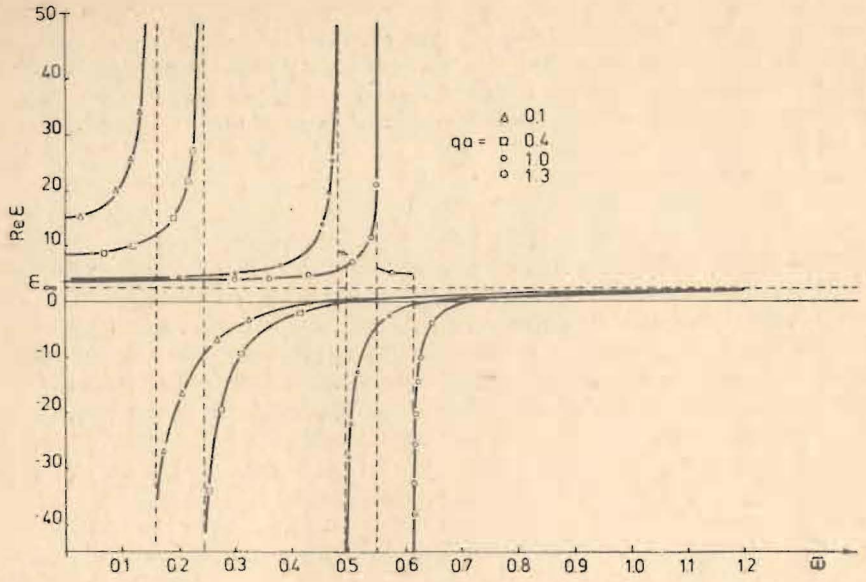

Fig.5. Real part of the DF versus frequency for different wave vectors ($\epsilon_\infty = 2.5$, C =0.45).

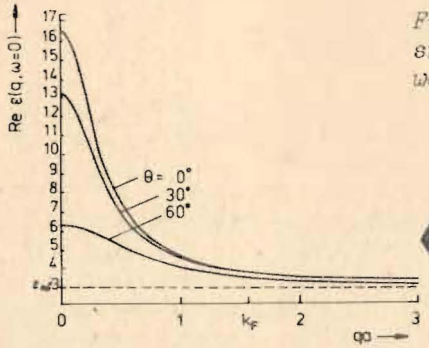

Fig.6. Static value of the DF versus wave vector (Θ is the angle between $\vec{q}$ and the chain axis).

ferent angles Θ. In comparison with usual semiconductors the DF along the chain direction shows strong spatial dispersion. At $q_\parallel = 2k_F = \pi/a$ we have

$$\mathrm{Re}\,\epsilon(q_\parallel = 2k_F,\ 0) = \epsilon_\infty + 4C\,(K - E)/(\pi^2 k^2)$$

$$\approx \underset{y \to 0}{\epsilon_\infty} + 4C\,(\ln(4/y) - 1)/\pi^2 \to \infty \qquad (4.23)$$

reflecting the giant Kohn-anomaly connected with the Peierls-transition.

5. CONCLUSIONS

In this paper the full DF for a two-band model was calculated in the RPA neglecting local field and exchange effects as well as some overlap terms (eq.(3.6)). Although the considered model is rather simple the obtained dependence of $\epsilon(\vec{q}, \omega)$ on the wave vector and the interchain coupling is non-trivial. All of the approximations made can be relaxed without serious problems at the expense of enhanced numerical efforts. Before the next step in this direction one should in our opinion compare the present approximation with the experiment, e.g., with the electron-loss spectroscopy data. However, due to the lack of monocrystals at the present time the morphology of polyacetylene films, especially the fibre structure have to be taken into account and for comparison with experiments additional considerations are necessary. We shall return to this problem in a forthcoming paper [15] dealing with the loss function and some other applications. It will be shown that the present model gives a good qualitative description of some features of the loss function and related quantities for comparatively low frequencies $\lesssim$ 7-8 eV. Using the obtained results some parameters of the 3D-generalized-SSH-model can be estimated from the experimental data.

ACKNOWLEDGEMENTS

We would like to thank Prof.G.Lehmann (Dresden) and A.S.Brazovskii (Moscow) for stimulating interest and discussions. Further thanks for discussions with H.Eschrig (Dresden) and W.Streitwolf (Berlin) for directing our attention to ref. [10].

APPENDIX

Starting from (4.1) simplified expressions for $\mathrm{Re}\,\epsilon(0, \omega)$ at certain frequencies (or special parameter range $y \ll 1$) are presented in this part. As is mentioned in the text, we use the following definitions and notation for the complete (incomplete) elliptic integrals of first, second and third kind, respectively

$$\left.\begin{aligned}
&F(\phi \backslash a) = \int_0^{\phi} (1 - \sin^2 a \sin^2\Theta)^{-1/2}\, d\Theta,\\
&F(\pi/2 \backslash a) \equiv K \approx \ln 4/y \quad \text{for} \quad y \ll 1,\ F(\tfrac{\pi}{2}, \tfrac{\pi}{2} - a) \equiv K',\\
&E(\phi \backslash a) = \int_0^{\phi} (1 - \sin^2 a \sin^2\Theta)^{1/2}\, d\Theta,\\
&E(\pi/2 \backslash a) \equiv E \approx 1 \quad \text{for} \quad y \ll 1,\ E(\tfrac{\pi}{2}, \tfrac{\pi}{2} - a) \equiv E',\\
&\Pi(n \backslash a) = \int_0^{\pi/2} (1 - n\sin^2\Theta)^{-1} (1 - \sin^2 a \sin^2\Theta)^{-1}\, d\Theta
\end{aligned}\right\} \qquad (A1)$$

In our problem the parameters n and α are given by

$$n = (1 - y^2)/(1 - \bar{\omega}^2), \quad \sin^2\alpha = k^2 = 1 - y^2. \tag{A2}$$

In the hyperbolic case ($n > 1$) it is useful to express $\Pi(n \backslash \alpha)$ by the Jacobi function (Zeta-function) $Z(\epsilon \backslash \alpha)$

$$\Pi(n \backslash \alpha) = -\delta_1 K Z(\epsilon_1 \backslash \alpha), \tag{A3}$$

$$Z(\epsilon_1 \backslash \alpha) = E(\epsilon_1 \backslash \alpha) - (E/K) F(\epsilon_1 \backslash \alpha), \tag{A4}$$

where

$$\delta_1 = [(1 - \bar{\omega}^2)\bar{\omega}^{-2}(\bar{\omega}^2 - y^2)^{-1}]^{1/2} \tag{A5}$$

$$\epsilon_1 = \arcsin[(1 - \bar{\omega}^2)/(1 - y^2)]^{1/2} \tag{A6}$$

In the circular cases ($n < 1 - y^2$, $0 < n < 1$) it is useful to introduce the Heuman function $\Lambda_0(\epsilon_2 \backslash \alpha)$ (Lambda-function)

$$\Pi(n \backslash \alpha) = K + (\pi/2)\,\delta_2 (1 - \Lambda_0(\epsilon_2 \backslash \alpha)), \tag{A7}$$

$$\Lambda_0(\epsilon_2 \backslash \alpha) = (2/\pi)\{KE(\epsilon \backslash \pi/2 - \alpha) - (K - E) F(\epsilon \backslash \pi/2 - \alpha)\}, \tag{A8}$$

where

$$\epsilon_2 = \arcsin[(1 - n)/\cos^2\alpha]^{1/2} = \arcsin[(1 - (\bar{\omega}/y)^2/(1 - \bar{\omega}^2)]^{1/2}, \tag{A9}$$

$$\delta_2 = [n(1 - n)^{-1}(n - \sin^2\alpha)]^{1/2} = [(1 - \bar{\omega}^2)(1 - (\bar{\omega}/y)^2)]^{1/2}/(\bar{\omega} y). \tag{A10}$$

In the second case mentioned ($n < 0$) one has to substitute

$$N = (\sin^2\alpha - n)(1 - n)^{-1} = (1 - y^2)\bar{\omega}^2/(\bar{\omega}^2 - y^2) \tag{A11}$$

and use the identity

$$\Pi(n \backslash \alpha) = (-n \cos^2\alpha)(1 - n)^{-1}(\sin^2\alpha - n)^{-1}\,\Pi(N \backslash \alpha) + \sin^2\alpha\,(\sin^2\alpha - n)^{-1} K. \tag{A12}$$

At very low frequencies $\bar{\omega} \ll y$ ϵ_2 approaches $\pi/2$ and it is convenient to introduce the small expansion parameter ψ by the relation

$$\tan\psi = \operatorname{cosec}\alpha \cdot \cot\epsilon = (\bar{\omega}/y)(1 - (\bar{\omega}/y)^2)^{-1/2} \tag{A13}$$

Rewriting (A8) in terms of

$$E(\epsilon \backslash \pi/2 - \alpha) = -E(\psi \backslash \pi/2 - \alpha) + E' + y^2 \sin\epsilon_2 \sin\psi, \tag{A14}$$

$$F(\epsilon \backslash \pi/2 - \alpha) = -F(\psi \backslash \pi/2 - \alpha) \tag{A15}$$

and using (A1), and the Legendre identity ($EK' + E'K - KK' = \pi/2$) we obtain for $\Pi(n \backslash \alpha)$ at $\bar{\omega} \ll y$

$$\Pi(n \backslash \alpha) = E/y^2 + (\bar{\omega}^2/3y^2)(2E/y^2 - 2E - K) + O((\bar{\omega}/y)^4). \tag{A16}$$

From (A16) and (4.1) we get (4.10). In the limit $\bar{\omega} \to y - 0$ ϵ_2 vanishes whereas δ_2 diverges $\sim (y - \bar{\omega})^{-1/2}$ and one obtains (4.3). In the high frequency region ($\bar{\omega} > 1$) using (A11), (A12) we have

$$\Pi(n \backslash \alpha) = K(1 - \bar{\omega}^{-2}) + (y/\bar{\omega})^2 (1 - \bar{\omega}^2)(y^2 - \bar{\omega}^2)\,\Pi(N \backslash \alpha), \tag{A17}$$

$$\delta_2 = (\bar{\omega}/y)[((\bar{\omega}/y)^2 - 1)/(\bar{\omega}^2 - 1)]^{1/2} \tag{A18}$$

$$\epsilon_2 = \arcsin[(\bar{\omega}^2 - 1)(\bar{\omega}^2 - y^2)]^{1/2}. \tag{A19}$$

Hence it is evident that in the limit $\bar{\omega} \to 1 + 0$ ϵ_2 and Λ_0 vanish whereas δ_2 diverges as $(\bar{\omega} - 1)^{-1/2}$. Using (A17), (A18), (A7) and (4.1) we obtain (4.3). At very high frequencies, i.e., $\bar{\omega} \gg 1$ from (A17)-(A19) it follows that

$$\Pi(n \backslash \alpha) \approx K + O(1/\bar{\omega}). \tag{A20}$$

So, we get (4.8). Finally, we consider the case of frequencies in the range of the interband transitions, i.e., $y \leq \bar{\omega} \leq 1$. Using formula [18]

$$\Pi(\sin^2\alpha, \alpha) = \sec^2\alpha E = E/y^2 \tag{A21}$$

the limit $\bar{\omega} \to y + 0$, i.e., (4.4) is easily evaluated. At the upper IBT-edge, i.e., at $\bar{\omega} \to 1 - 0$ it is seen from (A5-6) that δ_1 and ϵ_1 vanish, therefore we have

$$\Pi(n \backslash \alpha)\big|_{\bar{\omega} \to 1-0} = -(1 - \bar{\omega}^2)(F - E)/k^2 \tag{A22}$$

and $\operatorname{Re}\epsilon(0, \bar{\omega} \to 1 - 0)$ yields (4.6).

REFERENCES

1. Ritsko J.J. Phys.Rev., 1982, B26, p.2192; Ritsko J.J.et al. Phys.Rev.Lett., 1980, 44, p.1351.
2. Zscheile H. et al. phys.stat.sol.(b), 1984, 121, K161.
3. Fincher C.R. at al. Phys.Rev., 1980, B20, p.1589.

4. Vardeny Z., Orenstein J., Baker G.L. J.de Physique, 1983, 44 (b), C3-325.
5. Bernard O. et al. J.de Physique, 1983, 44 (b), C3-345.
6. Su W.P., Schrieffer J.R., Heeger A.J. Phys.Rev., 1980, B22, p.2099.
7. Brazovskii S.A., Matveyenko S.L. Zhurn.Eksp.Teor.Fiz., 1981, 81, p.1542.
8. Lee T.K., Kivelson S. Phys.Rev., 1984, B29, p.6687.
9. Hicks J.C., Wassermann A.L. Phys.Rev., 1984, B29, p.808.
10. Schulz H.J. Phys.Rev., 1978, B18, p.5756.
11. Maki K., Nakahara M. Phys.Rev., 1981, B23, p.5005.
12. Tinka Gammel J., Krumhansl J.A. Phys.Rev., 1981, B24, p.1035.
13. Kivelson S. et al. Phys.Rev., 1982, B25, p.4173.
14. Mintmire J.W., White C.T. Phys.Rev., 1983, B27, p.1447.
15. Drechsler S.L., Bobeth M. Submitted to phys.stat.sol.(b).
16. Hanke W. Adv.Phys., 1978, 27, p.287; Phys.Rev., 1975, B12, p.4501.
17. Fincher C.R.et al. Phys.Rev.Lett., 1982, 48, p.100; Baughman R.H., Moss G. J.Chem.Phys., 1982, 77, p.6321.
18. Grant P.M., Batra I.P. J.de Physique Coll., 1983, C3-44, p.437.
19. Abramowitz M., Stegun I. "Handbook of Mathematical Functions", National Bureau of Standards, Appl.Mathem.Ser., 1964, 55.
20. Dzyaloshinsky I.E., Kats E.J. Zh.Eksp.Teor.Fiz., 1968, 55, p.338 (Sov.Phys. - JETP, 1969, 28, p.178).
21. Williams P.F., Bloch A.N. Phys.Rev., 1974, B10, p.1097.
22. Ovchinnikov A.A., Ukrainskii I.I. Fiz.Tverd.Tela (Sov. Solid State Phys.), 1971, 16 (11), p.3239.
23. Alder S. Phys.Rev., 1962, 126, p.413.
24. Baeriswyl D., Maki K. Phys.Rev., 1983, B28, p.2068.

Дрекслер Ш.Л., Бобет М. E17-85-236

Диэлектрические свойства трансполиацетилена.
Приближение случайных фаз для макроскопической продольной диэлектрической проницаемости для полупроводника типа Пайерлса-Фролика с соизмеримостью 2

Вычисляется макроскопическая продольная диэлектрическая проницаемость /МПДП/, зависящая от волнового вектора и частоты, для полупроводника типа Пайерлса-Фролика с одним электроном на атом в рамках трехмерного приближения Ли и Кивельсона[8] основанного на модели Су-Шриффера-Хигера. Пренебрегаем эффектами локального поля и обмена, как и перекрытием волновых функций при определении матричных элементов зарядовой плотности. Приводятся условия для существования межзонных плазмонов, которые удовлетворены для trans $-(CH)_x$. Особое внимание уделяется изучению зависимости от $\vec{q}$ и от интеграла межцепочного перескока МПДП.

Работа выполнена в Лаборатории теоретической физики ОИЯИ.

Препринт Объединенного института ядерных исследований. Дубна 1985

Drechsler S.L., Bobeth M. E17-85-236

Dielectric Properties of Transpolyacetylene.
The Macroscopic Longitudinal Dielectric Function of a Peierls-Fröhlich Semiconductor of Commensurability 2 within RPA

The macroscopic longitudinal wave-vector- and frequency-dependent dielectric function /MLDF/ of a Peierls-Fröhlich semiconductor with one electron per site is calculated within the 3D-approach of Lee and Kivelson[8] based on the Su-Schrieffer-Heeger model. Local field and exchange effects as well as overlap in the calculation of the matrix elements of the charge density are neglected. Conditions for the occurrence of an interband plasmon are presented, which are fulfilled in trans $-(CH)_x$. Special attention is focused on the $\vec{q}$-dependence of the MLDF and the influence of the interchain hopping.

The investigation has been performed at the Laboratory of Theoretical Physics, JINR.

Preprint of the Joint Institute for Nuclear Research. Dubna 1985